AIP | Review of Scientific Instruments

Response function of modulated grid Faraday cup plasma instruments

Alan Barnett and Stanislaw Olbert

Citation: Review of Scientific Instruments **57**, 2432 (1986); doi: 10.1063/1.1139089
View online: http://dx.doi.org/10.1063/1.1139089
View Table of Contents: http://scitation.aip.org/content/aip/journal/rsi/57/10?ver=pdfcov
Published by the AIP Publishing

Response function of modulated grid Faraday cup plasma instruments

Alan Barnett and Stanislaw Olbert

Massachusetts Institute of Technology, Cambridge, Massachusetts 02139

(Received 17 March 1986; accepted for publication 4 June 1986)

Modulated grid Faraday cup plasma analyzers are a very useful tool for making *in situ* measurements of space plasmas. One of their great attributes is that their simplicity permits their angular response function to be calculated theoretically. In this paper we derive an expression for this response function by computing the trajectories of the charged particles inside the cup. We use the Voyager plasma science (PLS) experiment as a specific example. Two approximations to the "rigorous" response function useful for data analysis are discussed. The theoretical formulas were tested by multisensor analysis of solar wind data. The tests indicate that the formulas represent the true cup response function for all angles of incidence with a maximum error of only a few percent.

INTRODUCTION

Since the earliest days of space exploration, space probes have included instruments to measure plasma particles. There are two broad classes of plasma instruments: the modulated grid Faraday cup and the electrostatic analyzer. Modulated grid Faraday cups consist of a collector and several grids. The operation of such detectors is the topic of the bulk of this paper. Electrostatic analyzers typically consist of two curved conducting plates, with a potential difference between them and a particle counter at one end. When particles enter the instrument, only those particles moving in the proper direction with the proper energy per charge reach the collector. A good review article on techniques of deep-space plasma measurements is by Vasyliunas.[1]

The first successful American spacecraft to carry a plasma probe was Explorer 10, launched in 1961. This instrument, which was the first to provide direct evidence of the existence of the solar wind[2] (it actually measured the flow in the magnetosheath), was a modulated grid Faraday cup. The existence of the solar wind was confirmed and became generally accepted after observations made by Mariner 2, which carried an electrostatic analyzer.[3]

As more missions were flown, the plasma instruments improved. In order to measure the solar wind direction, Faraday cups with segmented collector plates were flown. If the plasma flow direction differs from normal to the cup, the current to the individual segments differs because of the shadow of the aperture. Faraday cups with three segments were flown on Mariners 4 and 5, which were three-axis stabilized spacecraft,[4,5] while a cup with its collector divided into two segments was flown on each of the spin-stabilized spacecraft Pioneers 6 and 7 [6,7] and Explorer 33.[8]

Improved sensitivity to the flow angle can be obtained by using an array of Faraday cups, each of which is pointed in a different direction. An instrument consisting of an array of four Faraday cups which was flown on the Voyager missions to the outer planets[9] is shown in Fig. 1. This instrument has successfully measured positive ions and electrons in the solar wind[10] and at Jupiter[11,12] and Saturn.[13] For the case of a cold beam of particles (such as the solar wind) flowing in a direction close to the look direction of the cups, data analysis from these instruments is straightforward. For cases when either the flow direction is not close to the look direction of the cups, the plasma thermal speed is comparable to or greater than the bulk velocity, or both, detailed knowledge of the instrument response function is required for the data analysis. The full response function described below has already been used for the study of the plasma flow around the Io flux tube,[14] and further work utilizing it is in progress.

In this paper we discuss the operation of this type of instrument and derive an expression for its response function. Although the formulas which we quote describe the Voyager instrument, the method we use can easily be applied to any Faraday cup.

The response function of the cup is defined as the ratio of the particle flux reaching the collector to the particle flux incident on the aperture when the incident particles are a collimated, monoenergetic beam. We compute the response function by studying the trajectories of the particles inside the cup. In Sec. I we describe the model of the cup which we use and the nature of the approximations which we have to make.

We show that the response function can be written as a product of two terms: the "sensitive area" and the grid transparency. The sensitive area term is computed from a

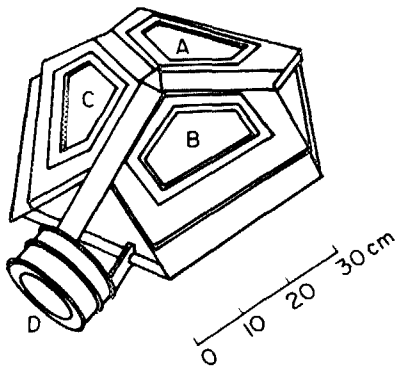

FIG. 1. Voyager plasma science (PLS) experiment, showing the relative orientations of the four cups.

 0034-6748/86/102432-09$01.30

straightforward study of the trajectories, while statistical arguments are required to determine the grid transparency term. These terms are derived in detail and explicit expressions for them are given for the case of the Voyager instruments in Sec. II and III.

Once the response function is known, one can use it to analyze data. The collector current from a plasma described by a known distribution function can be computed by performing an integration over velocity space. The problem of data analysis, therefore, becomes the problem of solving an integral equation for the distribution function. A very useful approximate method for solving the integral equation is to use a parameterized model for the distribution function and then find the "best fit" values for the parameters. In order to do this one must be able to perform the velocity space integration. Certain further approximations which permit the integration over the components of velocity perpendicular to the cup normal to be performed analytically for the case where the distribution function is a convected Maxwellian are described in Sec. IV.

Once we have computed the response function, we want to test it. In order to do this, one would like to have a very narrow test beam. Unfortunately, it is very difficult to make such a beam in the lab. We have used the calm solar wind at about 4 a.u. as our test beam. Analysis of data from Voyager 1 taken when the spacecraft was rotating (Voyager is a three-axis stabilized spacecraft) causing the solar wind to enter the cups at large angles indicates that our expressions are an excellent representation of the true response functions of the cups for all energies and angles of incidence. This analysis is discussed in Sec. V.

I. PHYSICS OF THE MODULATOR GRID FARADAY CUP

In this section we analyze the physics of the Faraday cup and present the model which we use to compute the response function, using the Voyager plasma science (PLS) instrument as an example. Throughout this paper we will consider the measurement of positive ions. For electrons, the analysis which we present can be modified in a straightforward manner, although in that case the emission of secondaries must be considered.

As can be seen from Fig. 1, the PLS instrument consists of four Faraday cups. Three of them, called the A, B, and C cups are arrayed about an axis of symmetry and have pentagonally shaped apertures and collectors. The fourth cup, called the D cup, is circular in shape (a more conventional design) and points 88° from the main sensor symmetry axis. The geometry will be very important for understanding the test of the response function.

A cross section of one of the PLS instrument's main sensor cups is shown in Fig. 2. The cup consists of an aperture stop, eight parallel grids, and a collector plate mounted in a metal housing. A top view of a cup is shown in Fig. 3. Figure 3 also defines a coordinate system which we call cup coordinates ($\hat{z}$ is the inward pointing cup normal). Notice that the collector is much larger than the aperture, a fact which gives this cup a much larger field of view than a conventional cup.

During operation, the collector plate and all of the grids except the modulator grids and the suppressor grid are grounded to the spacecraft. The suppressor grid is kept at -95 V to shield the collector from the plasma electrons and to return any secondary electrons to the collector. The instrument is used by applying a square-wave positive voltage to the modulator grids and measuring the collector current. Since more particles are repelled when the retarded potential is increased, the current waveform is an inverted square wave, as shown in Fig. 4. We call the upper and lower limiting modulator voltages ϕ_k and ϕ_{k+1}, respectively, and the corresponding collector currents I_k^* and I_{k+1}^*. The signal I_k is the amplitude of the current step, given by

$$I_k = I_k^* - I_{k+1}^* . \tag{1}$$

We wish to determine collector current as a function of the modulator voltage and the plasma distribution function. To a first approximation, the signal consists of all of the incident

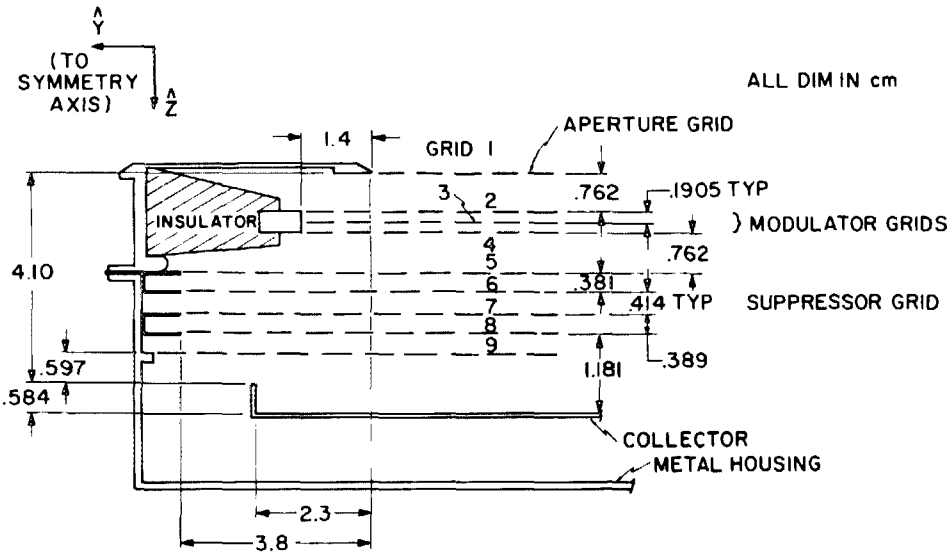

FIG. 2. Main sensor: vertical cut of upper segment. Cross section of a PLS main sensor cup. The grids are numbered 1–9, and the directions of $\hat{y}$ and $\hat{z}$ axes (cup coordinates) are shown.

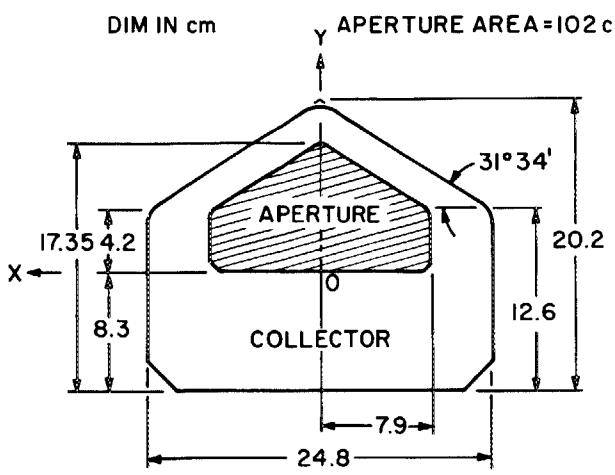

FIG. 3. PLS main sensor aperture and collector areas. Note direction of axes for cup coordinates: $\hat{z}$ points into the cup.

particles for which the z component of velocity (v_z) is between v_k and v_{k+1}, where v_k is related to ϕ_k by

$$v_k = (2Z^* e\phi_k / A^* m_p)^{1/2}, \tag{2}$$

where m_p is the proton mass, A^* is the mass of the ion in amu, Z^* is the charge state of the ion, and e is the proton charge. To obtain a better approximation, we need to study the motion of the charged particles inside the cup.

The total electric current incident on the aperture (I_{ap}) due to ionic species a is

$$I_{ap} = Z_a^* e \iint_{\text{Aperture}} dx\, dy \int_{-\infty}^{\infty} dv_x \int_{-\infty}^{\infty} dv_y \times \int_0^{\infty} v_z f_a(\mathbf{v})\, dv_z , \tag{3}$$

where $dx\,dy$ is an area element in the aperture, and $f_a(\mathbf{v})$ is the distribution function of ion species a. For the total current, one must sum over all species. In the remainder of this paper we will suppress the subscript a.

Not all of the particles incident on the aperture reach the collector. In principle, given the initial position and velocity of a particle, one can calculate its trajectory and thereby determine whether or not it will reach the collector. Therefore, we can formally write for the collector current

$$I_k^* = Z^* e \iint_{\text{Aperture}} dx\, dy \int_{-\infty}^{\infty} dv_x \int_{-\infty}^{\infty} dv_y \times \int_0^{\infty} v_z f(\mathbf{v}) H(\mathbf{v}, x, y, \phi_k)\, dv_z , \tag{4}$$

where $H(\mathbf{v}, x, y, \phi_k)$ is equal to one if the trajectory of a particle incident on the aperture at the position x, y with velocity $\mathbf{v}$ reaches the collector, and is equal to zero otherwise. In practice, Eq. (4) is useless in this form, because the precision with which we can calculate the particle trajectories is insufficient to permit us to accurately predict whether or not a given incident particle will collide with one of the grids. We can, however, compute the *probability* that a particle will collide with a grid. If we denote by A_{ap} the area of the aperture and by $R(\mathbf{v}, \phi_k)$ the probability that an incident particle with velocity $\mathbf{v}$ has of reaching the collector (which is the same as the fraction of particles of a uniform beam of particles with velocity $\mathbf{v}$ which reaches the collector), we can rewrite the Eq. (4) as

$$I_k^* = Z^* e A_{ap} \int_{-\infty}^{\infty} dv_x \int_{-\infty}^{\infty} dv_y \int_0^{\infty} v_z f(\mathbf{v}) R(\mathbf{v}, \phi_k)\, dv_z . \tag{5}$$

We call $R(\mathbf{v}, \phi_k)$ the response function of the detector.

To determine R, we use the following model of the cup. We assume that the electrostatic potential inside the cup depends only on z and that it is a linear function of distance between any two adjacent grids. (The model potential for the Voyager PLS main sensor cups is shown in Fig. 5.) This approximation neglects the fine structure of the fields near the grid wires and the fringing fields near the edges of the grids. Since the distance between the grids is much greater than the spacing between the wires and the grid spacing is much smaller than the linear dimensions of the grid, this approximation should be adequate.

In our model field we can calculate the particle trajectories exactly. The particle trajectory between any two grids is either a straight line or a parabola. If we now assume that

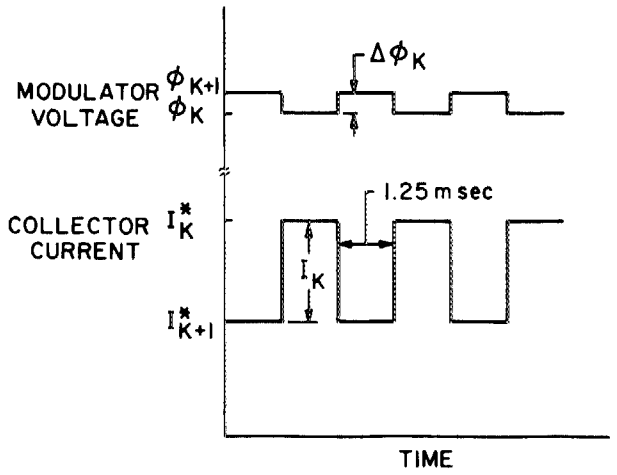

FIG. 4. Modulator voltage and collector current vs time. ϕ_k is the modulator grid threshold voltage of the k th channel, $\Delta\phi_k$ is the voltage width of the k th channel, I_k^* is the collector current when the modulator grid voltage is ϕ_k, and I_k is the current in the k th channel.

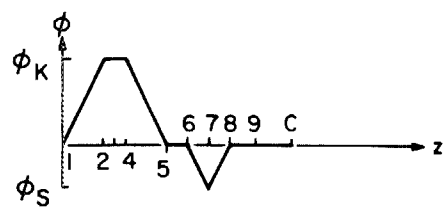

FIG. 5. Model potential vs z for a PLS main sensor cup. The numbered tick marks on the z axis correspond to the locations of the grids (see Fig. 2). The tick mark labeled c corresponds to the collector.

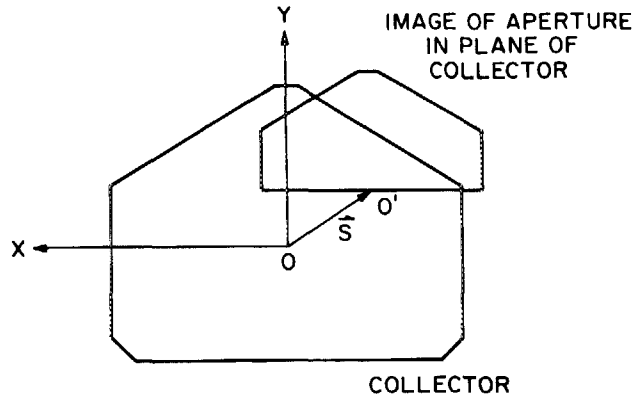

FIG. 6. Definition of the shift vector. The figure shows the outline of the collector of one of the main sensor cups, with the image of the aperture in the collector plane superposed on it. An incident monoenergetic beam of particles will have the shape of the aperture as it travels through the cup. The shift vector S is the vector which lies in the collector plane and points from the point directly underneath the center of the long side of the aperture to the corresponding point on the image of the aperture in the incident beam.

the probability of a particle striking a grid (a possibility not included in our trajectory calculation) does not depend on the position where the particle enters the cup, we can write R as a product of two terms and a normalization constant,

$$R(\mathbf{v}, \phi_k) = T(\mathbf{v}, \phi_k) A(\mathbf{v}, \phi_k)/A_{\text{ap}} , \tag{6}$$

where T is the transparency of the grids (the probability that a particle does *not* collide with a grid) and A is the "sensitive area" (the area of the aperture for which incident particles will strike the collector).

II. SENSITIVE AREA

We discuss first the sensitive area. Consider an incident beam of particles of velocity $\mathbf{v}$. If v_z is less than v_k, defined by Eq. (2), then the particle will be repelled by the modulator voltage, and so R will be 0. We take this into account by changing the lower limit of integration over v_z [in Eq. (5)] from zero to v_k.

If v_z is greater than v_k, then in the collector plane the beam will have the shape of the aperture, but its position will be displaced because of the components of the particle velocity transverse to the cup normal direction, as shown in Fig. 6. We define a two-dimensional vector S, also shown in Fig. 6, to be the displacement of the aperture image from a perpendicular projection of the aperture into the plane of the collector. One can calculate from the equations of motion that the "shift vector" S is given by

$$S_x = S^* h(v_x/v_z) , \tag{7a}$$

$$S_y = S^* h(v_y/v_z) , \tag{7b}$$

where h is the distance between the aperture and the collector and S^*, called the shift function, depends only upon v_z, the cup geometry, and the grid voltages. For the Voyager main sensor cups, the shift function is given explicitly by

$$S^* = 0.743 \left(\frac{[1 - (1 - v_k^2/v_z^2)^{1/2}]}{(v_k^2/v_z^2)} \right) + 0.093 \left(\frac{1}{1 - (v_k^2/v_z^2)} \right)^{1/2} + 0.392 \left(\frac{[(1 + v_s^2/v_z^2)^{1/2} - 1]}{(v_s^2/v_z^2)} \right) + 0.340 . \tag{8}$$

The subscript s refers to the suppressor grid; v_s is defined in a manner analogous to the definition of v_k in Eq. (2),

$$v_s = |2Z^* e\phi_s / A^* m_p|^{1/2} , \tag{9}$$

where ϕ_s is the voltage on the suppressor grid.

Once the shift vector is known, the sensitive area can be computed in a straightforward manner using a geometrical construction. For cups with cylindrical symmetry, the sensitive area depends only on the magnitude of S and the functional dependence can be expressed simply in closed form. For the Voyager main sensor, on the other hand, this functional dependence is complicated. As there are 16 separate regions where the dependence is different (see Fig. 7), an exact analytical representation is cumbersome. A plot of the sensitive area (normalized to unity for normal incidence) as a function of S_y/h, with S_x/h as a parameter, is shown in Fig. 8.

III. GRID TRANSPARENCY

We now consider the grid transparency. The transparency of a single grid is defined as the probability of an incident particle traversing the plane of the grid without colliding with the wires (all particles which strike the wires are assumed to be absorbed). We model a grid as a planar structure consisting of two perpendicular sets of parallel cylindrical wires. The transparency of the grid will be the product of the transparencies of each set of wires considered separately.

Consider a set of wires which run in the $\hat{y}$ direction (as before, $\hat{z}$ is taken to be normal to the plane of the grid). Since the transparency of these wires does not depend upon v_y, we

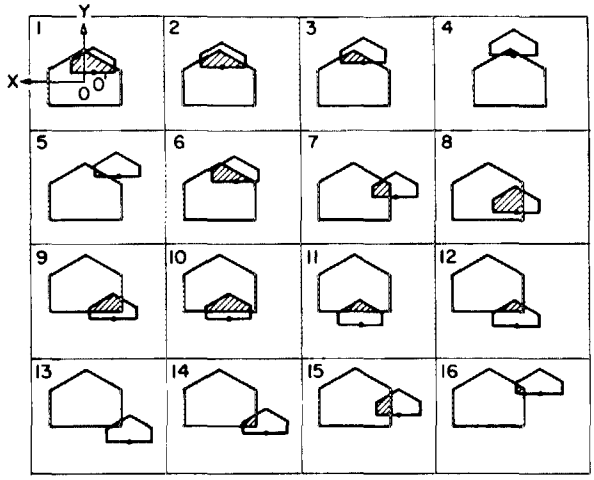

FIG. 7. Sensitive area of a main sensor cup. The figure shows the 16 distinct regions in which there is a different functional dependence of the sensitive area on the shift vector.

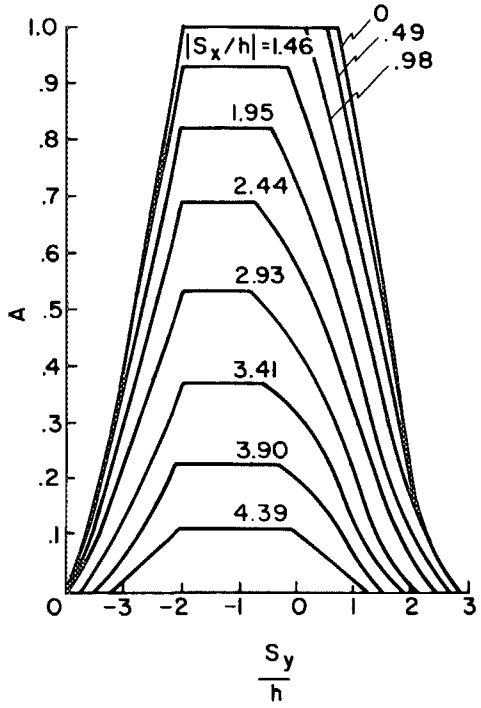

FIG. 8. Main sensor sensitive area vs S_y/h.

only need to consider the projection of the particle motion into the x-z plane. The probability of a particle colliding with one of the wires is simply the ratio of the area of the wires to the area of the gaps between the wires projected into a plane perpendicular to the particle velocity vector. As can be seen from Fig. 9, the probability of collision is proportional to $\sec\alpha$, where α is the angle between the projection of the particle velocity into the x-z plane and the z axis. The same line of reasoning can be applied to the set of wires which runs in the $\hat{x}$ direction. Using the computed trajectories in our simplified cup model to compute the value of α for each grid and noting that the probability of a particle reaching the collector plane without colliding with a grid is simply the product of the probabilities of it successfully traversing each individual grid, we can write the grid transparency term as the following product:

$$T=\prod_{i=1}^{N}\left[1-c\left(1+\frac{v_x^2}{v_z^2-2Z^*e\phi_i/A^*m_p}\right)^{1/2}\right]\times\left[1-c\left(1+\frac{v_y^2}{v_z^2-2Z^*e\phi_i/A^*m_p}\right)^{1/2}\right], \quad (10)$$

where ϕ_i is the voltage on the ith grid, c is the ratio of the wire diameter to the wire spacing, and N is the total number of grids.

For the voyager main sensor, $c=\frac{1}{42}$, and the sets of wires in the different grids are parallel. Since each cup has three modulator grids, one suppressor grid, and five grounded grids (see Fig. 1), the transparency is given explicitly by

$$T=\left[1-c\left(1+\frac{v_x^2}{v_z^2}\right)^{1/2}\right]^5\left[1-c\left(1+\frac{v_x^2}{v_z^2-v_k^2}\right)^{1/2}\right]^3\times\left[1-c\left(1+\frac{v_x^2}{v_z^2+v_s^2}\right)^{1/2}\right]\left[1-c\left(1+\frac{v_y^2}{v_z^2}\right)^{1/2}\right]^5\times\left[1-c\left(1+\frac{v_y^2}{v_z^2-v_k^2}\right)^{1/2}\right]^3\times\left[1-c\left(1+\frac{v_y^2}{v_z^2+v_s^2}\right)^{1/2}\right]. \quad (11)$$

For the Voyager main sensor cups at normal incidence, $T=T_0=(1-c)^{18}=0.65$.

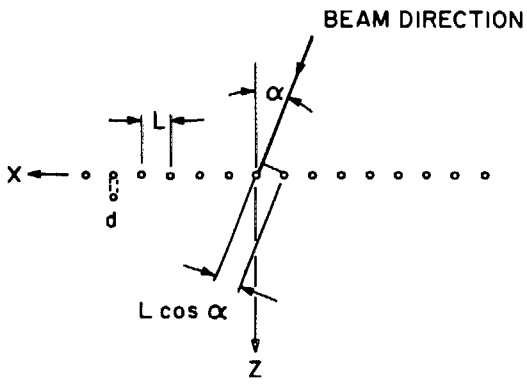

FIG. 9. Geometry for grid transparency calculation. A beam of particles incident on a grid of parallel, cylindrical wires is shown. α is the angle between the beam direction and the normal to the plane of the grid, L is the distance between the centers of two adjacent wires, and d is the wire diameter. The wires run in the $\hat{y}$ direction and the $\hat{z}$ direction is normal to the grid plane, with $+\hat{z}$ making an acute angle with the direction of the incident beam.

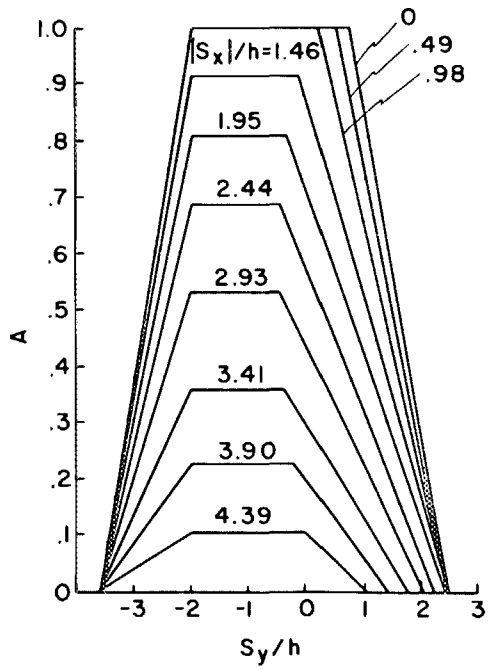

FIG. 10. Main sensor sensitive area vs S_y/h (trapezoidal approximation). Compare with Fig. 8.

IV. FURTHER APPROXIMATIONS

In order to use our results to analyze data, one must evaluate the integrals of Eq. (5) for a parameterized distribution function and use the data to obtain "best fit" values for the parameters. It is possible to do all of the integrations numerically, but a much faster running computer code can be written if some of the integrations can be done analytically. In this section we outline two approximation schemes which permit analytical, closed form evaluation of the integrations over v_x and v_y. The details of the schemes are given in Ref. 15.

For the complicated geometry of the Voyager PLS main sensor, a suitable analytical expression for the sensitive area (Fig. 8) must first be found. We used a family of trapezoids, plotted in Fig. 10. The formulas for these trapezoids are

$$A = A_x(S_x/h)A_y(S_x/h,S_y/h)\,, \tag{12a}$$

$$A_x = \frac{(S_x/h)+X_r'}{X_r'-X_r}\,, \quad -X_r' < S_x/h < -X_r\,, \tag{12b}$$

$$A_x = 1\,, \quad -X_r < S_x/h < X_r\,, \tag{12c}$$

$$A_x = -\frac{(S_x/h)-X_r'}{X_r'-X_r}\,, \quad X_r < S_x/h < X_r'\,, \tag{12d}$$

$$A_x = 0\,, \quad \text{otherwise}\,, \tag{12e}$$

$$A_y = \frac{(S_y/h)-Y_d'}{Y_d-Y_d'}\,, \quad Y_d' < S_y/h < Y_d\,, \tag{12f}$$

$$A_y = 1\,, \quad Y_d < S_y/h < Y_u(S_x)\,, \tag{12g}$$

$$A_y = \frac{(S_y/h)-Y_u'(S_x)}{Y_u(S_x)-Y_u'(S_x)}\,, \quad Y_u(S_x) < S_y/h < Y_u'(S_x) \tag{12h}$$

$$A_y = 0\,, \quad \text{otherwise}\,, \tag{12i}$$

with

$$X_r = 1.10\,, \tag{13a}$$

$$X_r' = 4.94\,, \tag{13b}$$

$$Y_d = -2.02\,, \tag{13c}$$

$$Y_d' = -3.62\,, \tag{13d}$$

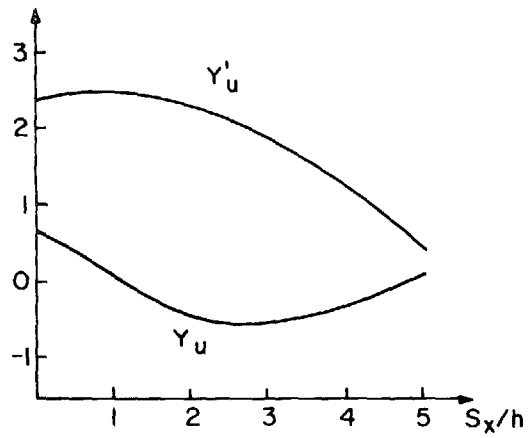

FIG. 11. Y_u and Y_u' vs S_x/h.

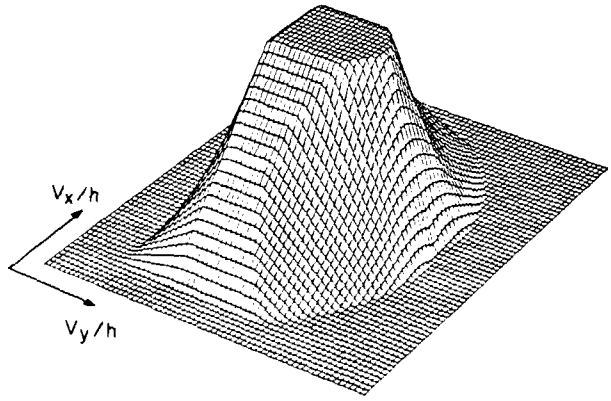

FIG. 12. Three-dimensional plot of the sensitive area vs S_x and S_y in the trapezoidal approximation.

$$Y_u = \frac{0.762\cos[1.018|S_x/h|+0.247]}{1+0.25|S_x/h|}\,, \tag{13e}$$

$$Y_u' = 2.50 - 0.125[|S_x/h|-1]^2\,. \tag{13f}$$

All of the quantities defined by Eq. (12b)–(12i) and (13a)–(13f) are dimensionless. Y_u and Y_u' are plotted in Fig. 11. Figure 12 shows a three-dimensional (3-D) plot of $A(S/h)$. The values of X_r, X_r', Y_d, Y_d', Y_u, and Y_u' were chosen to match the volume of the solid of Fig. 12 as closely as possible with the volume of the solid representing the true area overlap. Figure 13 shows a 3-D plot of $R(S_x/h,S_y/h)$, computed using the "trapezoidal approximation" for A and Eq. (11) for T.

We shall now proceed to describe two different approximation schemes. In both cases the plasma distribution function will be assumed to be a convected Maxwellian,

$$f(\mathbf{v}) = \frac{n_0}{w^3\pi^{3/2}}\exp[-(\mathbf{v}-\mathbf{V})^2/w^2]\,, \tag{14}$$

where $\mathbf{V}$ is the plasma bulk velocity, w is the thermal speed, and n_0 is the particle number density. For the case where $V \gg w$, we have a well-collimated beam. In this case we can approximate the dependence of f on v_x and v_y by a product of delta functions

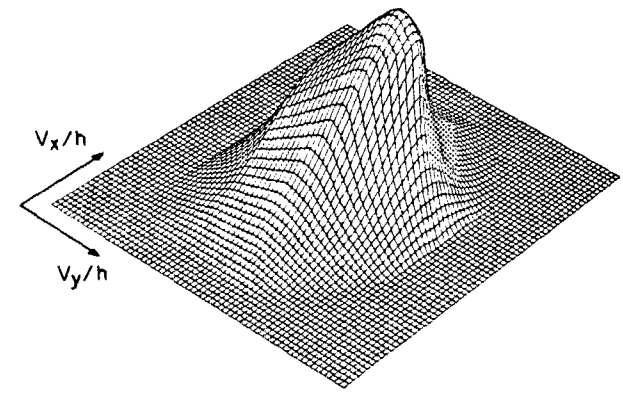

FIG. 13. Three-dimensional plot of the full response function, computed using the trapezoidal approximation for the sensitive area and the "exact" expression for the grid transparency.

$$f(\mathbf{v}) = \frac{n_0}{w\sqrt{\pi}}\,\delta(v_x - V_x)\delta(v_y - V_y) \times \exp[-(v_z - V_z)^2/w^2]\,. \quad (15)$$

The delta functions permit the integrations over v_x and v_y to be computed trivially, leaving only the numerical integration over v_z. This approximation was used to experimentally test the response function, as described in the following section.

For the more general case where the bulk velocity is not much greater than the thermal speed, we must change the form of the expression for the grid transparency. It is possible to approximate Eq. (10) by an expression of the form

$$T = \left\{\sum_{i=1}^{2} c_i \exp\left[-a_i\left(\frac{v_x}{v_z}\right)^2\right]\right\} \times \left\{\sum_{j=1}^{2} c_j \exp\left[-a_j\left(\frac{v_y}{v_z}\right)^2\right]\right\}, \quad (16)$$

where the a's and c's are functions of the grid voltages and v_z only. The values of the a's and c's must be determined by a numerical fitting procedure. This approximation permits the desired integrals to be evaluated numerically with the aid of the saddle point method.

For a cylindrically symmetrical cup, a similar approximation scheme can be used. This case is much simpler, since the response function does not depend upon the azimuthal angle of incidence of the particles. (This is so except for a small effect due to the rectangular structure of grids themselves. If the grids are mounted such that the wires of a given grid are not parallel to the wires of the other grids, this effect will be minimized.) The sensitive area can be approximated by a single trapezoid, and the grid transparency term contains one sum of Gaussians, rather than the product of two sums of Gaussians. The integration over azimuth angle then yields a modified Bessel function, which can be approximated by a sum of exponentials to permit analytic evaluation of the integral over the magnitude of the tangential velocity. The response function of the D cup of the Voyager PLS instrument is discussed in detail in Ref. 15.

V. EXPERIMENTAL TEST OF THE RESPONSE FUNCTION

In order to test our theoretical response function, we have analyzed data taken by Voyager 1 during a cruise maneuver. Voyager is a three-axis stabilized spacecraft, and most of the time it is oriented such that the main sensor symmetry axis, which is parallel to the spacecraft's main antenna, is pointed toward the Earth. Since the angular separation between the Earth and the sun, as viewed from the outer solar system, is small, the solar wind direction was usually almost parallel to the main sensor symmetry axis. In this configuration the "unity response" approximation to the cup response (all incident particles which are not stopped by the modulator voltage reach the collector, but the aperture area is corrected for the transparency of the grids at normal incidence) is good. During the cruise maneuver,

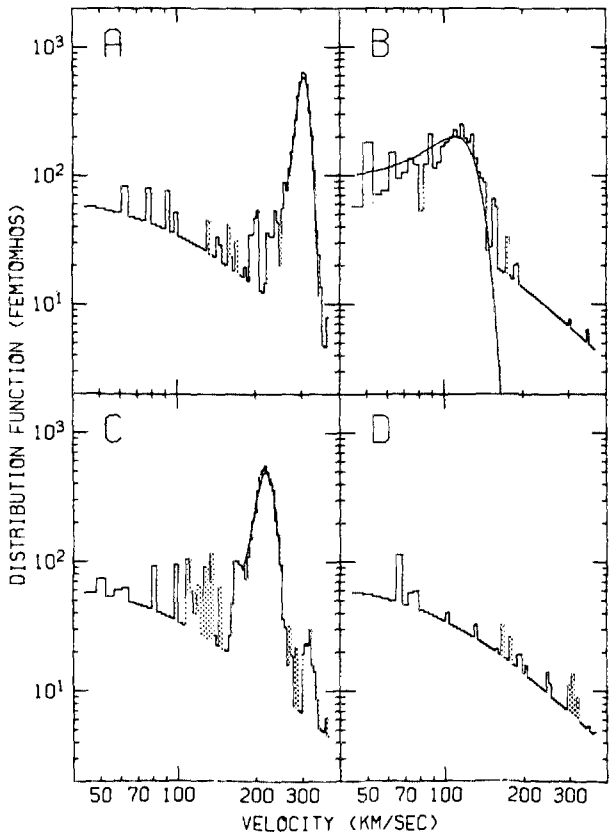

FIG. 14. Reduced distribution function vs velocity for cruise maneuver spectrum 1. The staircases are the data, while the smooth curve is the fit.

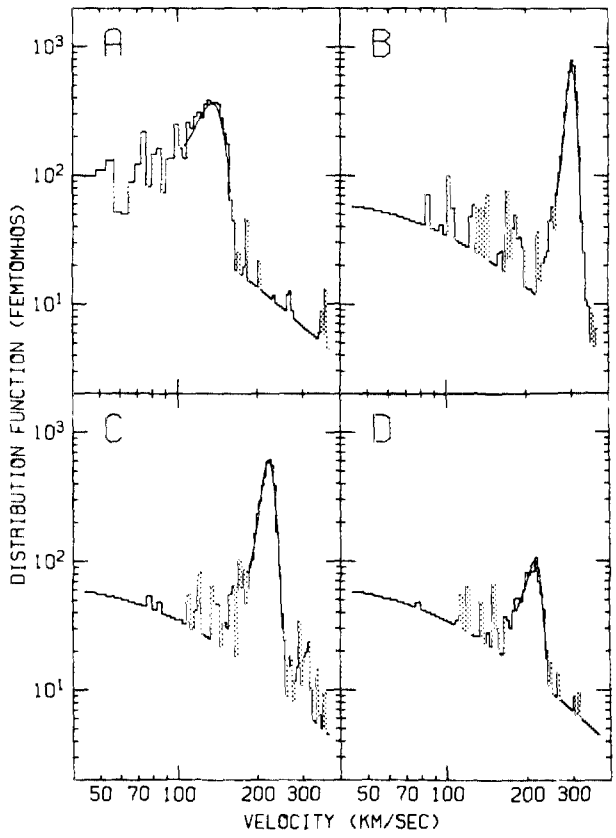

FIG. 15. Reduced distribution function vs velocity for cruise maneuver spectrum 2. The staircases are the data, while the smooth curve is the fit.

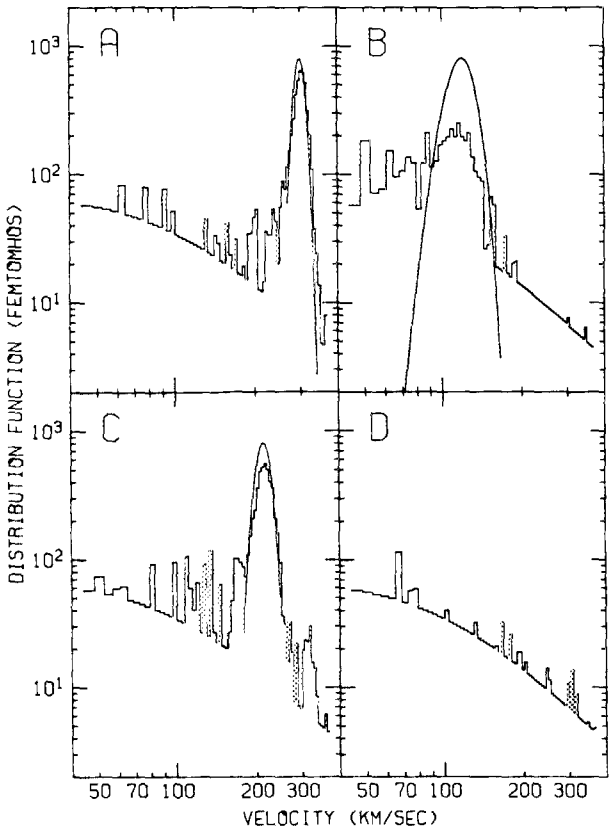

FIG. 16. Reduced distribution function vs velocity for cruise maneuver spectrum 1. The staircases are the data, while the smooth curve is a simulation done assuming "unity" response using the plasma parameters determined from the fit which is plotted in Fig. 14. Note that the locations of the peaks in the simulation are correct, but their heights and shapes are wrong.

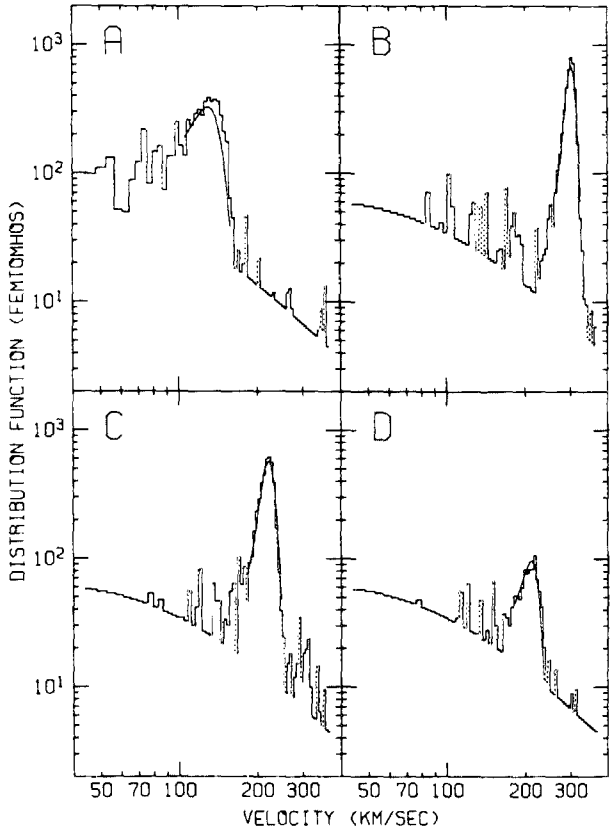

FIG. 17. Reduced distribution function vs velocity for cruise maneuver spectrum 2. The staircases are the data, while the smooth curve is the fit. The change in the orientation of the spacecraft between the time of the peaks in the different cups was *not* compensated for. Compare to Fig. 15.

however, the spacecraft performed a series of rotations, some of which involved rotating the main antenna away from the Earth.

The data were taken over a period of 90 min on 14 September 1978, when Voyager 1 was 4.1 a.u. from the sun. The solar wind bulk speed during the maneuver varied between 368 and 378 km/s, while the thermal speed varied between 14 and 20 km/s. Data were taken simultaneously in all four cups. Two such spectra are shown in Figs. 14 and 15. The figures consist of $I_k/(\phi_{k+1} - \phi_k)$ plotted versus v_k for each cup. The staircases are the data, while the smooth curves are the "best fit" simulations. The fits are excellent, correctly reproducing the location, height, and shape of each peak in all of the cups in which there is a signal. For the spectra of Fig. 14, the angles between the bulk velocity and the cup normals for the A, B, C, and D cups were 38°, 72°, 56°, and 124°, respectively, while for the spectrum of Fig. 15 the angles were 67°, 34°, 52°, and 56°, respectively.

As an illustration of the extent to which we are actually testing our response function using this process, consider Figs. 16 and 17. Figure 16 is the same spectrum as Fig. 14, except that the smooth curve is a simulation using the parameters derived from the fit of Fig. 14 with the assumption of unity response. Notice that although the peaks are all in the right place because of the effect of the sharply peaked distribution function, the heights and shapes are all wrong. It should be pointed out that the current in the B cup of this spectrum is only about 4% of what the current would be if the same beam were at normal incidence.

An even more striking example is shown in Fig. 17. While the measurements were being taken, the spacecraft was rotating at a rate of one rotation every 33 min. Since the instrument takes 0.24 s to measure a single channel, and the same channel is measured simultaneously in all four cups, the peak in the B cup (channel 46) was measured about 5 s after the peak in the A cup (channel 24) was measured. During that time, the spacecraft rotated about 0.9°. For the fit shown in Fig. 15, this rotation was compensated for, while for the fit shown in Fig. 17 the effect of this small rotation was neglected. Our theoretical response function is sufficiently good that failure to account for this rotation of less than 1° made the fit noticeably worse! The quality of the fits to the data taken during the cruise maneuver has convinced us that our theoretical response function represents the true response function of the Voyager PLS experiment within a few percent for all angles of incidence.

ACKNOWLEDGMENTS

We would like to thank H. Bridge, J. Belcher, and A. Lazarus for helpful discussions. This work was supported under Jet Propulsion Laboratory JPL Contract No. 953733 and NASA Contract NSG 22-009-015.

[1]V. M. Vasyliunas, in *Methods of Experimental Physics*, edited by R. A. Lovberg (Academic, New York, 1971), Vol. 9B, p. 49.
[2]H. S. Bridge, C. Dilworth, A. J. Lazarus, E. F. Lyon, B. B. Rossi, and F. Sherb, I. G. Bull. **55**, 12 (1962).
[3]M. Neugebauer and C. W. Snyder, Science **138**, 1095 (1962).
[4]A. J. Lazarus, H. S. Bridge, J. M. Davis, and C. W. Snyder, in *Space Research VII*, edited by R. L. Smith-Rose (North-Holland, Amsterdam, 1965), p. 1296.
[5]H. S. Bridge, A. J. Lazarus, C. W. Snyder, E. J. Smith, L. Davis, Jr., P. J. Coleman, Jr., and D. E. Jones, Science **158**, 3809, 1665 (1962).
[6]A. J. Lazarus, H. S. Bridge, and J. Davis, J. Geophys. Res. **71**, 15, 3787 (1966).
[7]A. J. Lazarus, G. L. Siscoe, and N. F. Ness, J. Geophys. Res. **73**, 7, 2399 (1968).
[8]E. Lyon, A. Egidi, G. Pizzella, H. S. Bridge, J. Binsack, R. Baker, and R. Butler, in *Space Research VIII*, edited by A. P. Mitra, L. G. Jacchia, and W. S. Newman (North Holland, Amsterdam, 1968), p. 99.
[9]H. S. Bridge, J. W. Belcher, R. J. Butler, A. J. Lazarus, A. M. Mavretic, J. D. Sullivan, G. L. Siscoe, and V. M. Vasyliunas, Space Sci. Rev. **21**, 259 (1977).
[10]P. R. Gazis and A. J. Lazarus, Geophys. Res. Lett. **9**, 4, 431 (1982).
[11]F. Bagenal and J. D. Sullivan, J. Geophys. Res. **86**, A10, 8447 (1981).
[12]R. L. McNutt, J. W. Belcher, and H. S. Bridge, J. Geophys. Res. **86**, A10, 8314 (1981).
[13]A. J. Lazarus and R. L. McNutt, J. Geophys. Res. **88**, 11, 8831 (1983).
[14]A. S. Barnett, J. Geophys. Res. **91**, A3, 3011 (1986).
[15]A. S. Barnett, NASA Technical Report No. CSR-TR-84-1, 1984.